Electronic Supplementary Information

Single-cell-array biomass templated architecture of hierarchical porous electrocatalysts for Zn-air and Zn-H$_2$O$_2$ batteries

Zhenjiang Zhu [a], Liangyu Jin [a], Meng Zhou [a], Kui Fu [a], Fancheng Meng [a], Xiangfeng Wei [a], Jiehua Liu*[,a,b]

a Future Energy Laboratory, School of Materials Science and Engineering, Hefei University of Technology Hefei 230009, China

b Key Laboratory of Advanced Functional Materials and Devices of Anhui Province, Engineering Research Center of High-Performance Copper Alloy Materials and Processing, Ministry of Education, Hefei 230009, China.

*Email: liujh@hfut.edu.cn and liujh@iccas.ac.cn

Experimental sections

Chemicals

Cobalt (II) acetate tetrahydrate was purchased from Sigma. Pt/C (20 wt %), and RuO$_2$ were purchased from Macklin. The other reagents are analytical grade and are used without any further purification.

Pre-processing of nori

To remove water-soluble impurities, nori slices were alternately soaked in deionized water and ethanol several times. The colorless nori was centrifuged out of ethanol and dried at 60 ºC.

Synthesis of ZIF-67/nori

The obtained colorless nori (1.0 g) was added into 0.04 mol/L cobalt acetate aqueous solution (40 mL) to absorb Co(II) ions (nori-Co^{2+}). Then, nori-Co^{2+} was added to the other 40 mL solution with 0.53 g 2-methylimidazole. ZIF-67/nori was obtained after a hydrothermal reaction at 120 °C for 6 hours.

Synthesis of ZIF-67/nori-derived catalyst

KOH (0.20 g), melamine (0.20 g), and ZIF-67/nori (0.20 g) were mixed and added into crucibles. The samples were annealed at 700, 800, and 900 °C for 3 h in N$_2$ atmosphere (heating rate 3 °C/min), respectively. After being washed with water, the obtained ZIF-67/nori-derived catalysts were named ZIF-67/nori-700, ZIF-67/nori-800, and ZIF-67/nori-900, respectively. ZIF-67/nori-R1 was obtained as the condition of ZIF-67/nori-800 except melamine

Materials characterizations

The samples were subjected to XRD testing by a D/MAX2500V diffractometer with Cu-Kα radiation. FESEM and TEM images were obtained by SU8020 (HITACHI) and JEM 2100F. N$_2$ adsorption-desorption isotherms were performed on an autosorb-IQ3 analyzer at 77 K. XPS measurements were performed by ESCLAB250 with a monochromatic Al Ka X-ray source with the power of 150 W. Raman spectra were collected by using Lab Raman HR Evolution.

Electrochemical measurements

Electrochemical measurements were performed on three-electrode cells at room temperature using an electrochemical workstation (CHI760E and DH7000) and a rotating disk electrode. 20% Pt wire and KCl-saturated $Hg/HgCl_2$ electrodes were used as counter and reference electrodes, respectively. Activity evaluations were performed in a 0.1 M KOH electrolyte system. Rotating disk electrode (RDE) measurements were performed using glassy carbon (GC) disks. Before testing, the GC discs were polished to avoid contamination. The catalyst ink was prepared by adding 5 mg of the resulting catalyst and 40 µl of Nafion solution (5 wt%, DuPont) to 960 µl of water/isopropanol (3:1) solvents. After ultrasonic treatment for 30 minutes, a homogeneous suspension was obtained. The 5 µl catalytic ink is then applied to the surface of the GC disk and dried at room temperature.

Before ORR evaluation, the CV curves in O_2-saturated KOH were obtained at a scan rate of 20 mV s^{-1}. The ORR LSV curves were obtained at different rotation speeds (400, 800, 1,200, 1,600, and 2,000 rpm) at a scan rate of 5 mV s^{-1} in an O_2-saturated 0.1 M KOH electrolyte. The OER LSV curves were recorded at a scan rate of 5 mV s^{-1} at 1,600 rpm in an O_2-saturated 1 M KOH electrolyte. The K–L equation (Equation S1) is applied to investigate the ORR kinetic.

$$\frac{1}{J} = \frac{1}{J_K} + \frac{1}{J_D} = \frac{1}{nFAkC_{O_2}} + \frac{1}{0.2nFAC_{O_2}D_{O_2}^{2/3}v^{-1/6}\omega^{1/2}}$$

(S1)

where J, J_K, and J_D represent electrode current density, dynamic current density, and diffusion limiting current density, respectively; n is the number of electron transfers per O_2 molecule; F is Faraday's constant with a Value of 96485 C mol^{-1}; k is the electron transfer rate constant; C_{O2}, D_o, and V is the oxygen concentration in the electrolyte, the diffusion coefficient of oxygen molecules and the kinematic Viscosity of the electrolyte, respectively. In 0.1 M KOH, the oxygen concentration is 1.2×10^{-6} mol cm^{-3} and the diffusion coefficient is 1.9×10^{-5} cm s^{-1}, the kinematic Viscosity is 0.01 cm^2 s^{-1}, A is the electrode area, about 0.07068 cm^2, and ω is the electrode rotation speed.

Battery test

Zn-air and Zn-H$_2$O$_2$ batteries were tested using a homemade cell. Zn-H$_2$O$_2$ batteries were designed with the optimized container of H$_2$O$_2$ decomposition, avoiding that H$_2$O$_2$ from contacting the gas diffusion layer and improving the durability problem. The working electrode with the catalyst of 2 mg cm^{-2} was prepared by casting the above catalyst ink onto the carbon paper, and the polished Zn plate (0.2 mm thickness) was used as the anode. 6 M L^{-1} KOH solution was used as the electrolyte for primary Zn-H$_2$O$_2$ batteries. Hydrogen peroxide of 30% was used in Zn-H$_2$O$_2$ batteries. All battery tests were conducted by the Neware battery system. Activated carbon and ZIF-67/nori-800 samples were used as low-rate and high-rate catalysts for H$_2$O$_2$ decomposition, respectively.
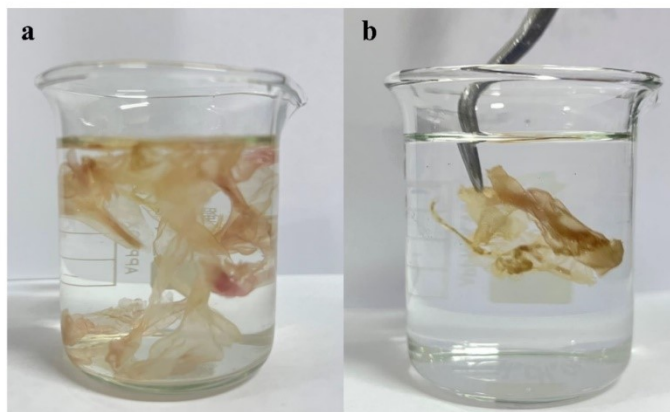
Fig. S1. Nori in deionized water (a) and ethanol (b).

After the nori cells are transferred from deionized water to ethanol, respiration occurs. The nori slices in deionized water swell and expand. However, when the nori slices in deionized water are transferred to ethanol, we find that the nori slices are dehydrated and the nori slices shrink.

Nori is single-cell-thickness biomass with a micro-cell-array sheet structure and natural macropores. Nori has the feature of respiration in ethanol/H$_2$O. In the inhalation process, the cytoplasm and organelles in nori cells can absorb water, which makes water passes through the cell membrane. Then the cytoplasm and organelles expand in nori cells (Fig. S1a). In the exhalation process, the cells could dehydrate because the water in cell diffuses easily into ethanol solution from cells.[S1,S2], when nori is put in ethanol (Fig. S1b). In the respiration process, the cells are purified due to

the removal of soluble impurities in nori cells, such as some inorganic salts and water organics.
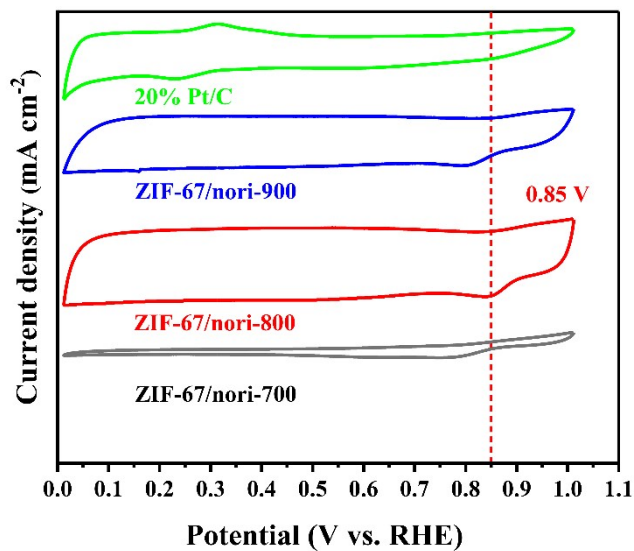

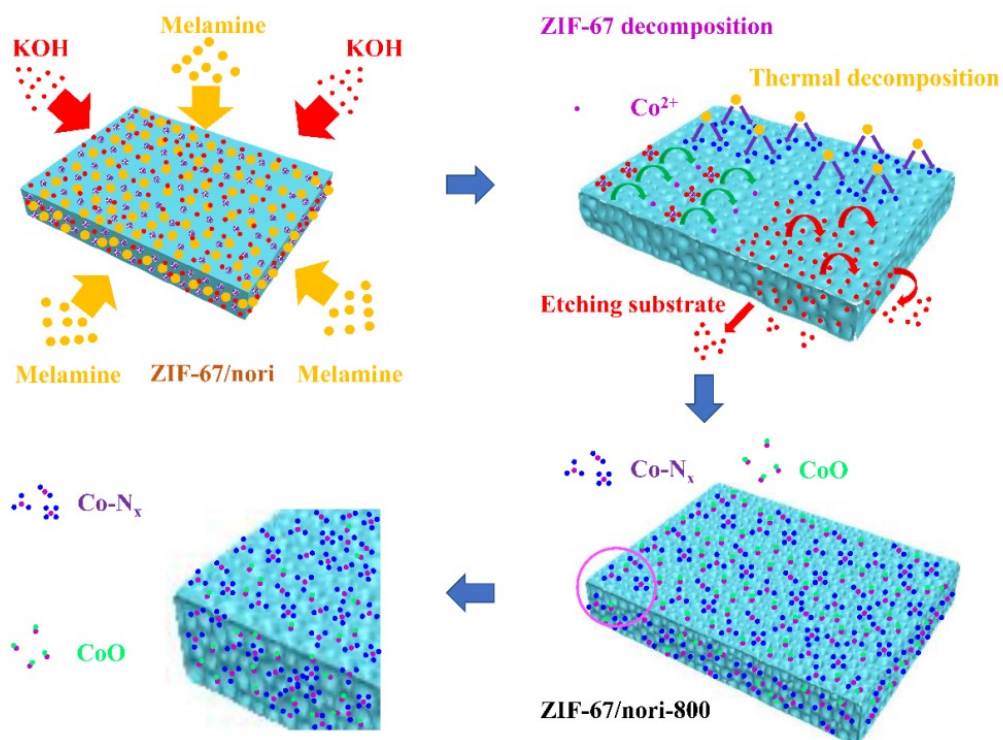**Fig. S2.** A CV test was performed under O_2 in 0.1 M L^{-1} KOH solution.

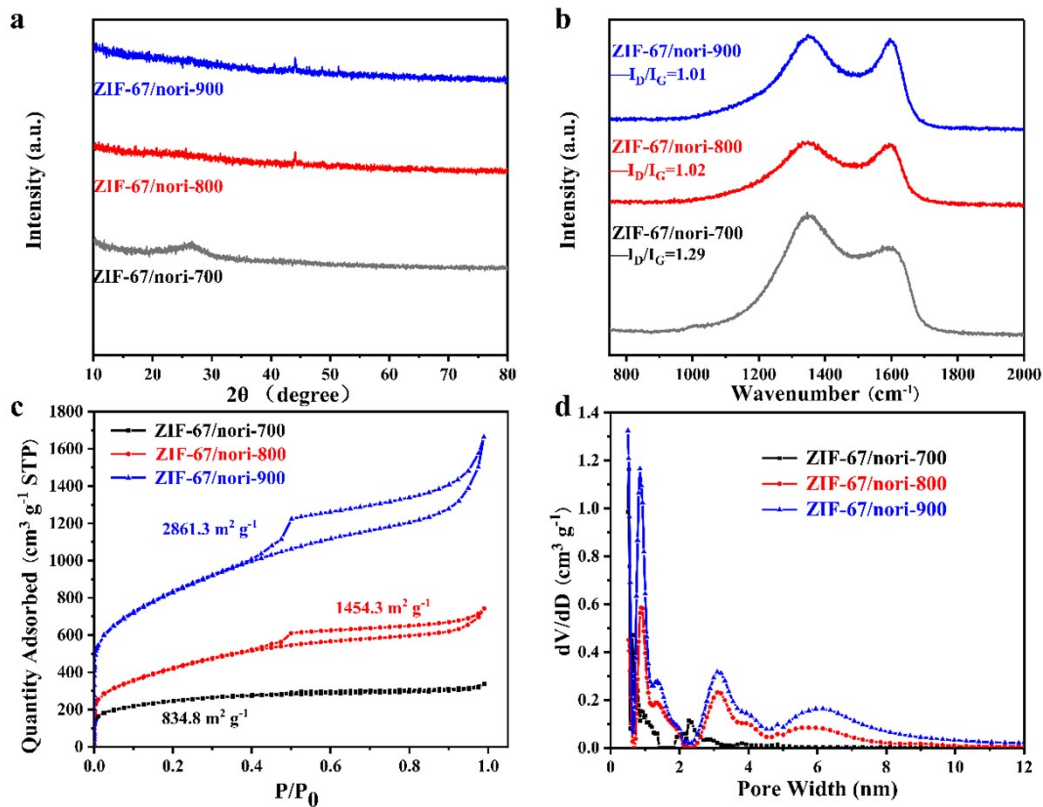**Fig. S3.** Preparation of ZIF-67/nori-800 from ZIF-67/nori.

Fig. S4. (a) XRD, (b) Raman, (c) N_2 adsorption-desorption isotherms, (d) The pore size distributions of ZIF-67/nori-derived catalysts.
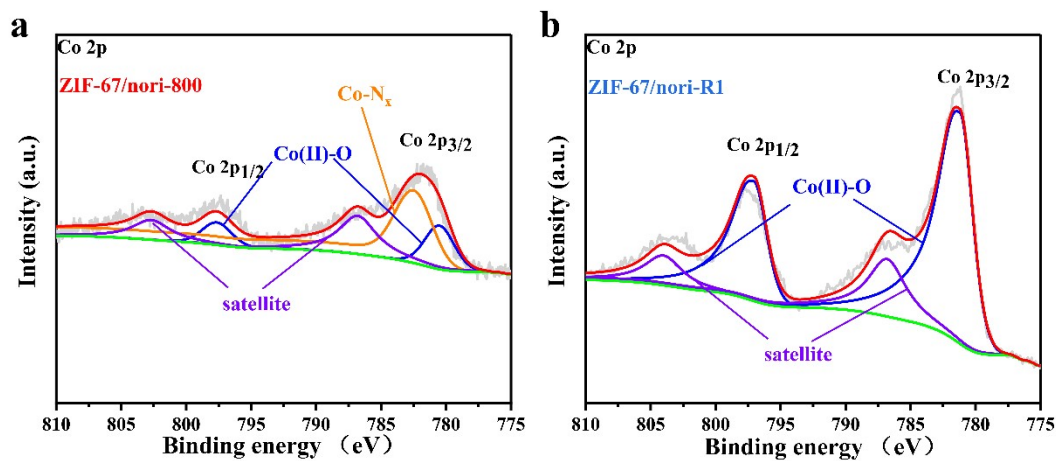

Fig. S5. High-resolution XPS spectra of Co2p of ZIF-67/nori-800 and ZIF-67/nori-R1.
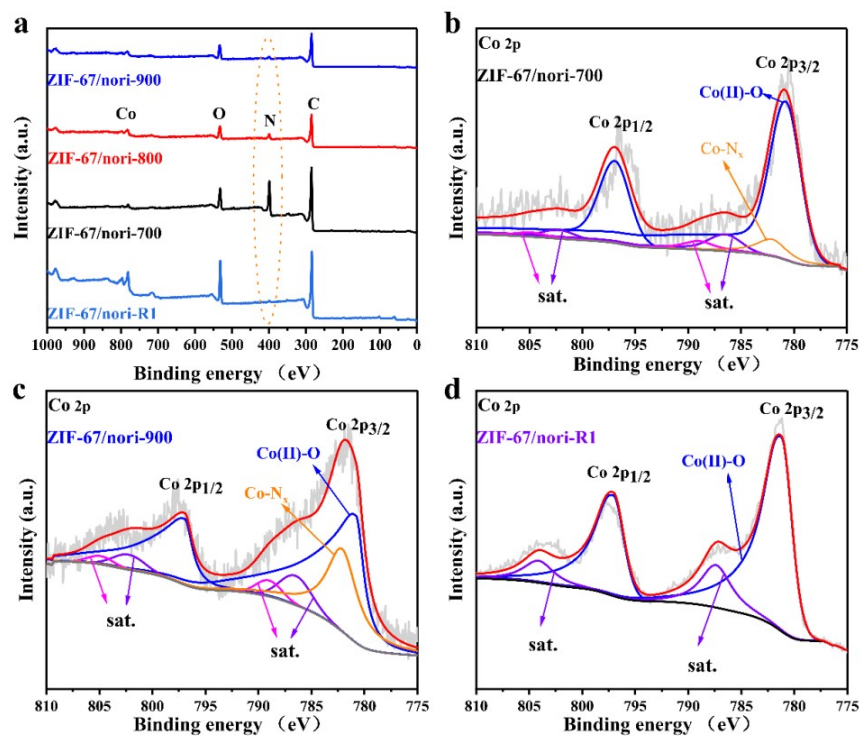
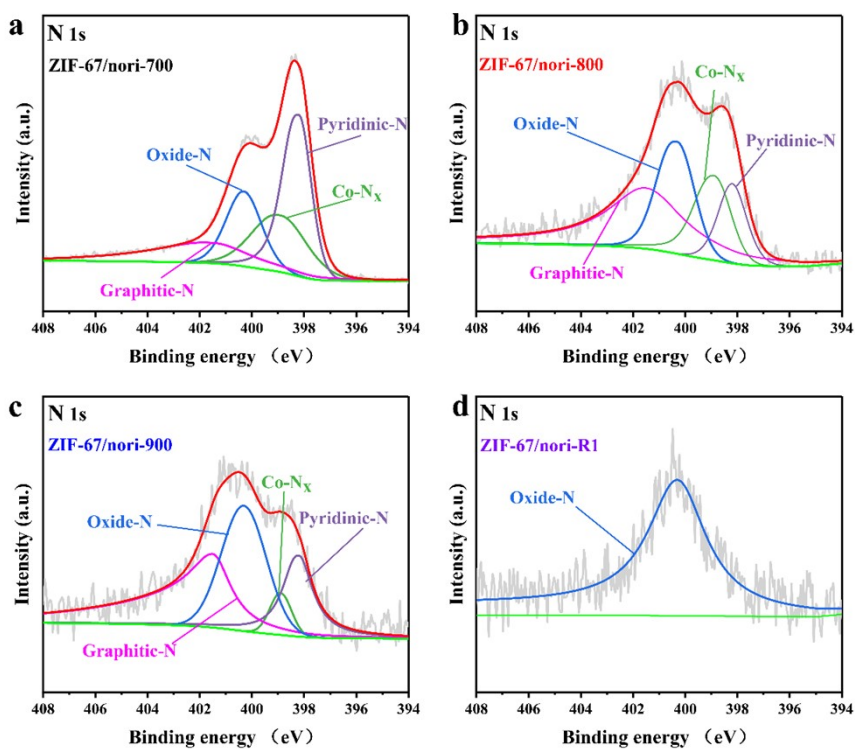**Fig. S6.** (a) XPS survey spectra, (b-d) High-resolution XPS spectra of Co2p of ZIF-67/nori-derived catalysts.

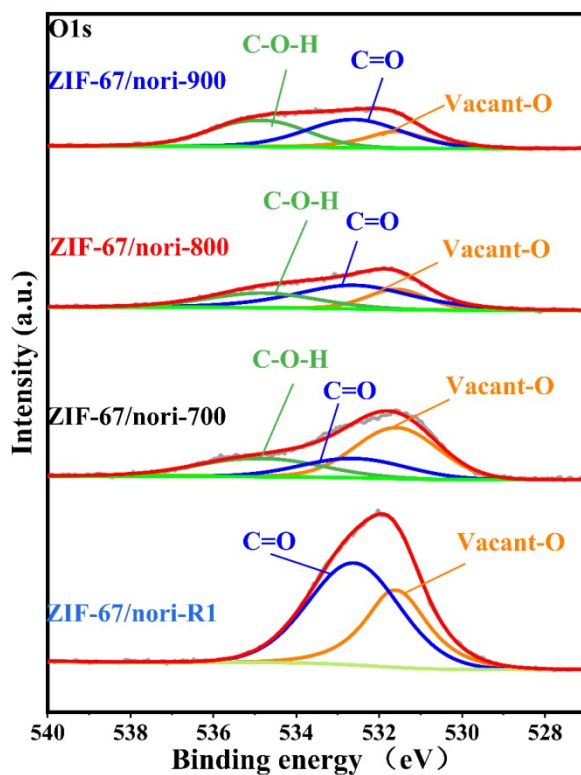**Fig. S7.** High-resolution XPS spectra of N1s of ZIF-67/nori-derived catalysts.

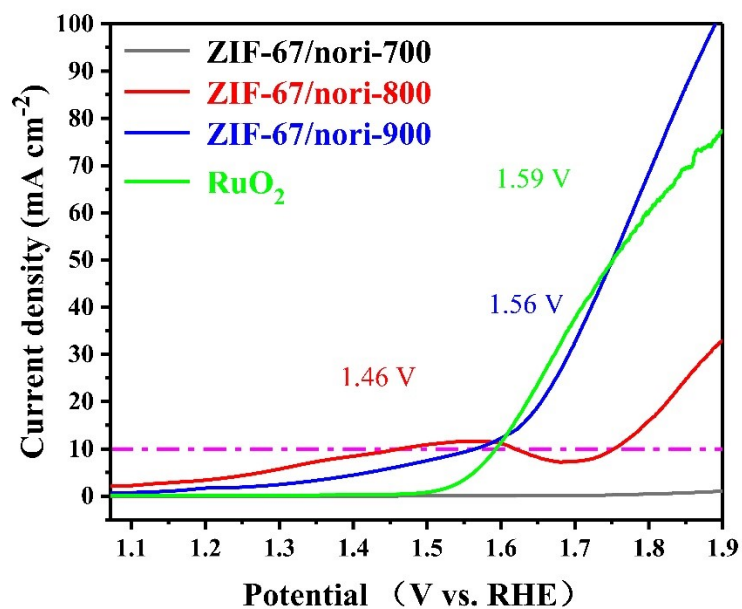**Fig. S8.** High-resolution XPS spectra of O1s of ZIF-67/nori-derived catalysts.

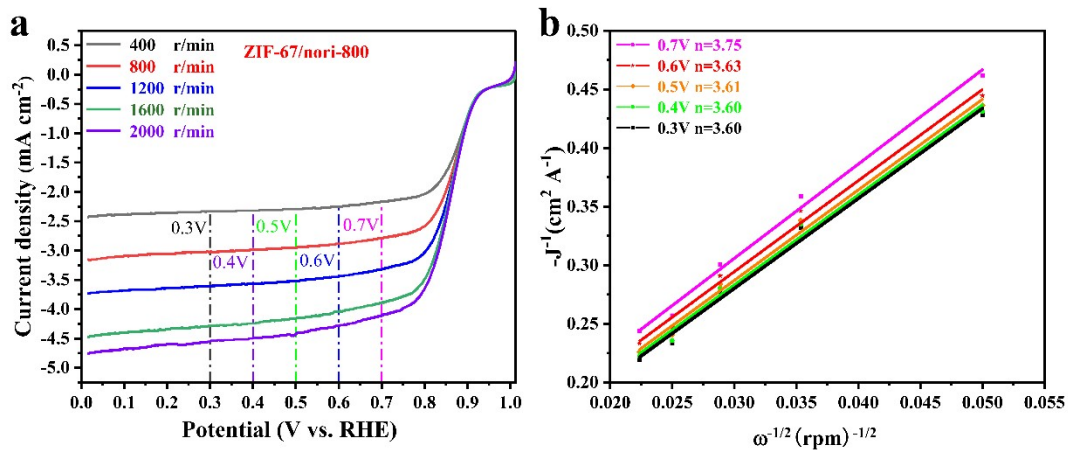**Fig. S9.** OER curves of ZIF-67/nori-derived catalysts and RuO$_2$

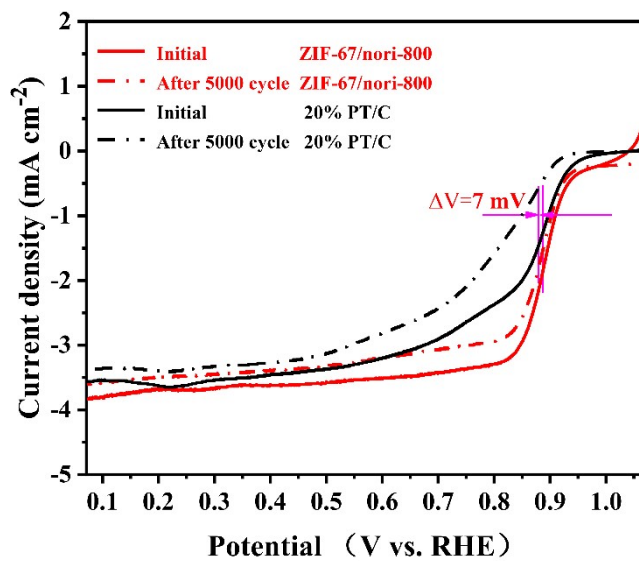**Fig. S10.** (a) LSV curves at different rotation speeds, (b) the K-L plots of ZIF-67/nori-800.

Fig. S11. LSV curves of the ZIF-67/nori-800 catalyst before and after 5000 cycles for the ORR.
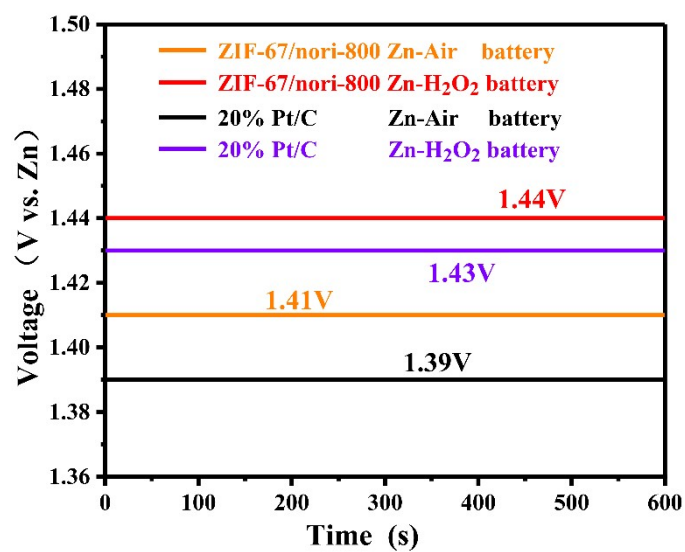
Fig. S12. Voc-t curves of Zn-H$_2$O$_2$ batteries and Zn-Air batteries with ZIF-67/nori-800 and 20% Pt/C as ORR catalysts.

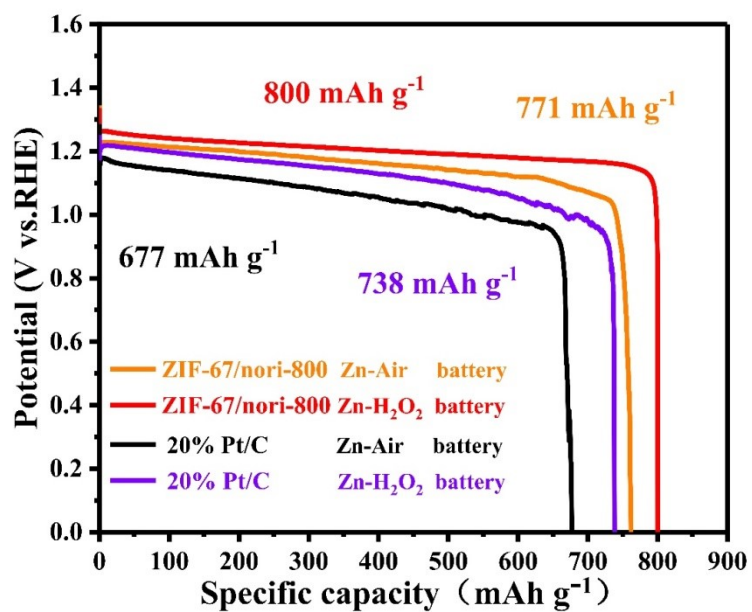**Fig. S13.** Specific capacity curves of Zn-air and Zn-H$_2$O$_2$ batteries with the Zn consumed using ZIF-67/nori-800 and 20% Pt/C as ORR catalysts.
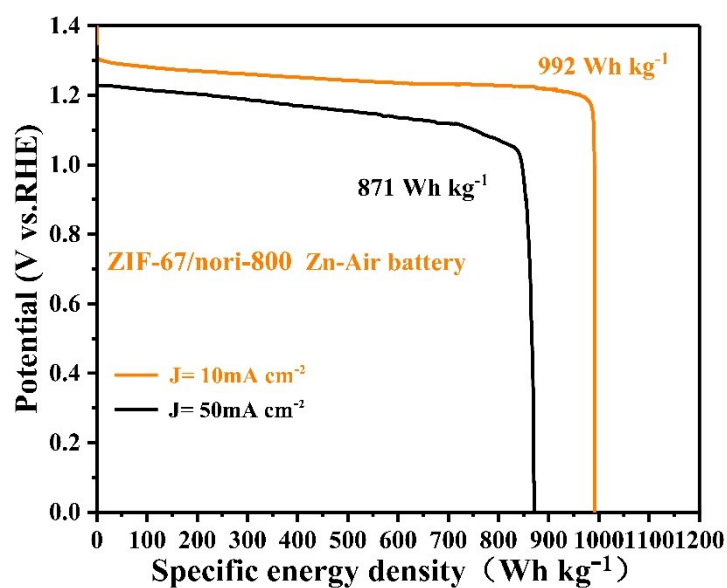
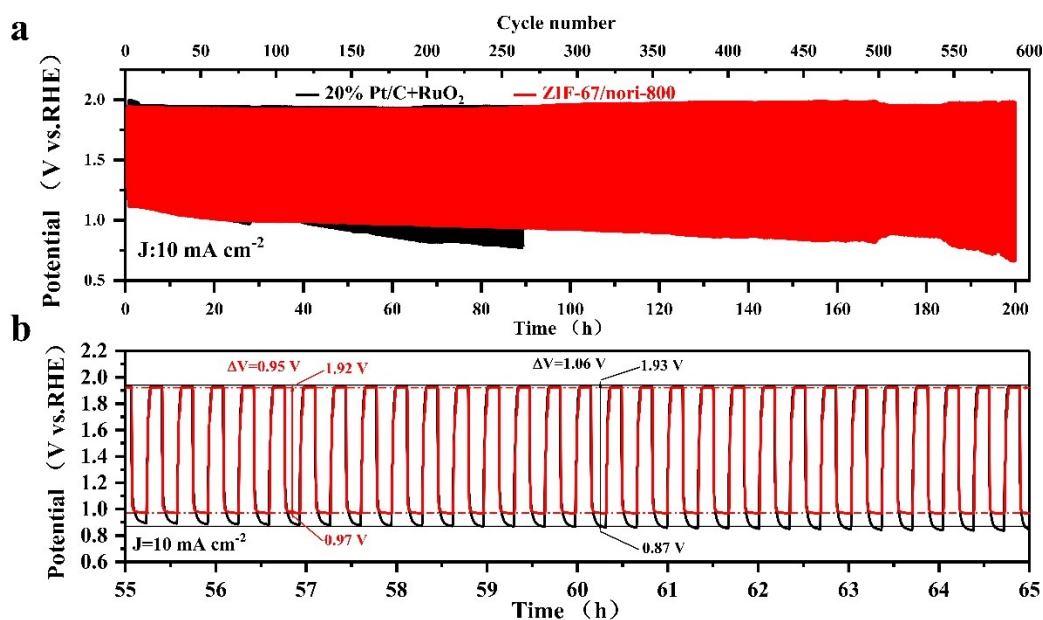**Fig. S14**. The specific energy density of Zn-air batteries using ZIF-67/nori-800 catalysts at 10 and 50 mA cm^{-2}.

Fig. S15. (a) Cycling performance of Zn-air batteries with ZIF-67/nori-800 and Pt/C+RuO$_2$, and (b) the detailed cycling performance at 55-65 hours.

Table S1. The presence of different atom ratios in the catalyst composites derived from XPS survey spectra.

Catalysts	C 1s at %	N 1s at %	O 1s at %	Co 2p at %
ZIF-67/nori-700	51.67	29.03	17.44	1.86
ZIF-67/nori-800	44.28	9.03	23.58	23.11
ZIF-67/nori-900	49.39	4.46	26.94	19.21
ZIF-67/nori-R1	40.59	1.59	27.54	30.28

Table S2. The atomic ratios of Co-N_x, Co(II)-O, and satellite peaks in the catalyst composites.

	ZIF-67/nori-700		ZIF-67/nori-800		ZIF-67/nori-900		ZIF-67/nori-R1	
	eV	At %	eV	At %	eV	At %	eV	At %
Co(II)-O Co 2p3	780.5	0.37	780.5	2.95	780.5	8.14	781.22	16.34
Co(II)-O Co 2p1	796.4	0.3	797.64	1.54	797.64	4.15	797.06	8.36
sat.	786.8	0.04	786.8	4.42	786.8	2.23	787.38	3.73
sat.	802.7	0.02	802.7	2.29	802.7	0.45	804.11	1.85
Co-N_x	782.5	1.13	782.5	11.91	782.5	4.24		

Table S3. The atomic ratios of Co-N_x, pyridinic N, graphitic-N, and pyrrolic-N in the catalyst composites.

	Co-Nx		Pyridinic N		GraphiticN		Pyrrolic N	
	eV	At %	eV	At %	eV	At%	eV	At%
ZIF-67/nori-700	398.9	1.14	398.2	12.92	401.5	5.41	400.1	9.56
ZIF-67/nori-800	398.9	0.29	398.2	1.52	401.5	3.27	400.1	3.93
ZIF-67/nori-900	398.9	0.09	398.2	0.8	401.5	1.97	400.1	1.60
ZIF-67/nori-R1							400.1	1.57

Table S4. The atomic ratios of Vacant-O, C=O, and C-O-H in the catalyst composites.

	O 1s					
	Vacant-O		C=O		C-O-H	
	eV	At %	eV	At %	eV	At%
ZIF-67/nori-700	531.58	10.71	532.61	4.85	534.8	1.88
ZIF-67/nori-800	531.58	5.15	532.61	11.45	534.8	6.98
ZIF-67/nori-900	531.58	4.89	532.61	11.4	534.81	10.65
ZIF-67/nori-R1	531.58	9.98	532.61	17.57		

Reference

S1   W. Jiang, H. Pan, F. Wang, M. Jiang, X. Deng and J. Li, *Journal of Applied Phycology*, 2014, **27**, 243-248.

S2   A. K. J. Sallal, Nimer, N.A., *World Journal of Microbiology and Biotechnology* **10**, 187–190 (1994).